Stress-Dependent Permeability of Reservoir Rock and Its Influence on Well Flow Rate: Experiment and Simulation

Larisa Nazarova[1(✉)], Leonid Nazarov[1], and Nikita Golikov[2]

[1] Chinakal Institute of Mining, Siberian Branch RAS, 630091 Novosibirsk, Russia
lanazarova@ngs.ru

[2] Trofimuk Institute of Petroleum Geology and Geophysics, Siberian Branch RAS, 630090 Novosibirsk, Russia

Abstract. Thermobaric tests are performed on Bazhenov oil-bearing shale containing above 10% of kerogen in view to determine its rheological properties. The test specimen under a statistical axial load is heated stepwise at temperatures $T_n = 60$, 100 and 150 °C with measurements of height $H(t)$. The temperature is risen if relative velocity of H gets less than 0.05. Deformation of the specimen is described by Kelvin–Voigt model, within which the inverse problem is stated and solved to determine Young module E_n and effective viscosity η_n of rocks by $H(t)$. The results of solution are approximated by two-parameter exponential functions, $E = E(T)$ and $\eta = \eta(T)$ relationships are established.

The lab-scale test bench is designed and manufactured to study the relationship of granular geomaterials permeability versus stresses. A polyurethane measurement cell of parallelepiped shape is filled with sized sand; controllable vertical stress σ is applied to different sections of the top edge. The constant gas pressure p is created on one of vertical edges, while gas flow rate $Q(p, \sigma)$ is recorded on the opposite edge. The mathematical model of experimental is developed. Hypothesizing that permeability depends on effective stress according to the exponential law with coefficient β in index, the analytical solution is found to the problem on stationary filtration in a cell under a non-uniform stress state. The researchers propose the process for quantitative estimation of β based on minimization of the relative discrepancy functional between Q and the theoretical value of gas flow rate. It is appeared that β can be determined without reference to gas viscosity and an initial permeability of geomaterial packing. According to the present test results β magnitude used to reduce slightly with stress growth.

The poroelastic model describing evolution of geomechanical and hydrodynamic fields in a near-well zone was employed for comparative analysis of metering characteristics of a well in terms of the routine deformation and poroperm parameters of production oil-bearing beds. It is demonstrated that a disregard of the established empirical relationships of permeability versus effective stresses and temperature can result in an appreciable upward bias of oil production prediction.

V. I. Karev et al. (Eds.): *Physical and Mathematical Modeling of Earth and Environment Processes (2018)*, SPEES, pp. 93–106, 2019.
https://doi.org/10.1007/978-3-030-11533-3_10

Keywords: Porous and granular media · Rock · Reservoir · Filtration · Lab experiment · Stress-dependent permeability · Rheology · Temperature · Inverse problem

1 Introduction

Substantiation of the oil pool development conception, estimation of underground reservoir production characteristics, GIS data processing are items of the far from complete list of problems which solution rests on the reliable information on poroperm properties of rocks, and regularities of their variability in the course of deposit exploitation [1–3]. Cross-disciplinary evolution models of different-nature physical fields are applied to study deformation and mass transfer in the well environment [4–11]. Intercoupling of these fields is described by empirical relationships, established, as a rule, under laboratory conditions. The relations of rheological and poroperm properties of reservoir rock versus stresses [12–14] and temperature [15] can serve study cases of such dependences being occasionally of the dominant factor for flow characteristics of a well. The present paper deals with establishment of empirical relationships of permeability vs. stresses and temperature based on the laboratory data for different-type geomedia, as well as the effect of such relationships on flow characteristics of a well is assessed in the frame of the geomechanical-hydrodynamic model [16] of fracture-porous medium.

2 Experimental Investigation of Bazhenov Shale Rheological Properties at Different Temperatures

The world hydrocarbon reserves are mostly represented with problematic resource such as low-gravity oil and bitumen [17, 18]; oil deposit of Bazhenov formation being surely of the said type. Such oil fields are conventionally developed by the thermal oil-bed treatment with both positive and negative effects: fluid viscosity reduction is of positive value, while decrease in permeability owing to fall of deformation parameters of rocks with temperature rise is a negative after-effect [19, 20]. Bazhenov rock (bazhenite) series contain up to 10% of organic matter functioning as a binder, thereto, their mechanical characteristics tend to alter wildly under thermal treatment.

The research objective is to establish empirical relationships of bazhenite rheological properties versus temperature. Under investigation was a collection of five cylindrical specimens of radius R = 14 mm and height $H_0 = 35.8$ mm, sampled from Bazhenov formation (Salym petroleum deposit, West Siberia). The tests were executed at the original test bench (Fig. 1a), which design is presented in Fig. 1b. A specimen placed between two aluminium punches was charged to a tube-type furnace. The system was subjected to vertical compression by a load of $M = 23$ kg in mass, followed by a stepwise heating. The specimen temperature was controlled by a heat sensor (red line in Fig. 2), variations in height versus time $H(t)$ were recorded by a dial-test indicator (absolute precision being 1 μm). Given a relative variation in H for 12 h becoming less than 5%, the temperature was increased up to a magnitude of the follow-on level for a few minutes, therewith the specimen used to elongate because of the thermal expansion of the rock.

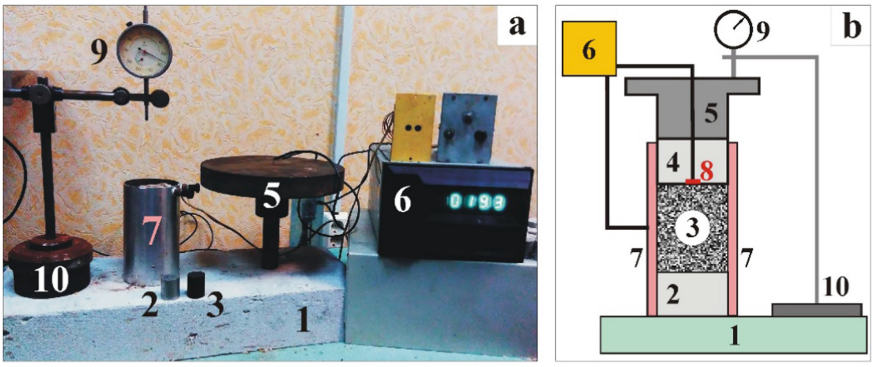

Fig. 1. Test bench (a) and experimental design (b): 1–heat-sealing base; 2, 4–bottom and top punches; 3–specimen; 5–load; 6–temperature-control module; 7–tube-type furnace; 8–heat sensor; 9–dial-test indicator; 10–stand.

Test data – variations in a relative height of the specimen $D(t) = H(t)/H_0$ – are shown by green circles in Fig. 2.

Let us consider axial strain

$$\varepsilon(t) = 1 - H(t)/H(t_n)$$

at successive time intervals $[t_n, t_{n+1})$ $(n = 1, 2, 3)$, where t_n – time moment when constant temperature T_n is reached in the test specimen (Fig. 2). In each of these intervals ε tends to a constant magnitude, so the deformation process can be described by Kelvin-Voigt viscoelastic model [21, 22]

$$E_n\varepsilon + \eta_n\dot{\varepsilon} = S, \quad \varepsilon(t_n) = 0, \tag{1}$$

where E_n and η_n are Young modulus and viscosity of geomaterial, respectively; $S = Mg/(\pi R^2)$ is constant stress applied to the specimen, g is gravity acceleration. Solution of (1) is

$$\varepsilon(t) = \varepsilon_n^r[1 - \exp(-E_n(t - t_n)/_n], \tag{2}$$

$\varepsilon_n^r = S/E_n$ is residual strain.

Let state the coefficient inverse problem: to find E_n and η_n from thermobaric test data (Fig. 2). Introduce the objective function

$$\Phi_n(E_n, \eta_n) = \frac{\sqrt{I_n \sum_i [\varepsilon(t_i, E_n, \eta_n) - \varepsilon_i]^2}}{\sum_i \varepsilon_i},$$

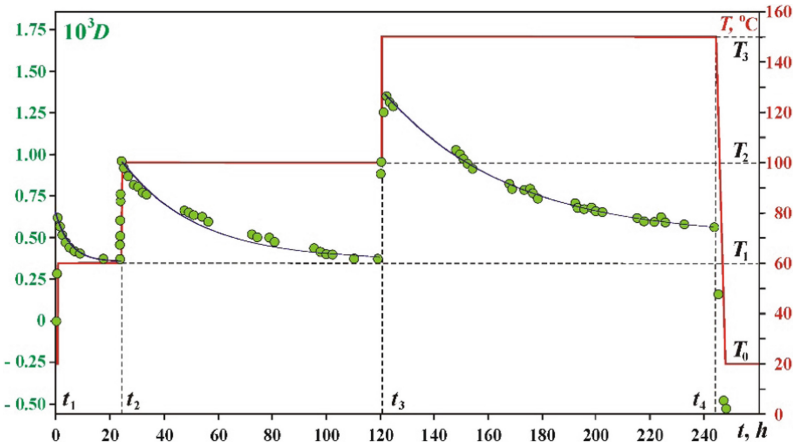

Fig. 2. Temperature graph and experimental data (Specimen 4).

where $\varepsilon(t_i, E_n, \eta_n)$ is a value of function (2) at some values of Young module and viscosity; input data $\varepsilon_i = 1 - H(t_i)/H(t_n)$ are calculated by a measured specimen height at moment t_i; summing is performed relative to i, for which $t_i \in [t_n, t_{n+1})$ (I_n – their amount, Table 1, line 2). A priory estimation of Young modulus $E_n^0 = SH_0/(H_0 - H_{min})$ (H_{min} – the minimum specimen height at the study time interval) is reported in Table 1 (line 3).

Table 1. Rheological properties of Specimen 4 at different temperatures.

	N	1	2	3
1	T_n, °C	60	100	150
2	I_n	11	36	52
3	E_n^0, MPa	211.5	66.0	50.8
4	E_n^*, MPa	220.6	59.8	47.1
5	η_n^*, TPa · c	1.48	7.38	7.95

According to numerical experiments, the objective functions are unimodal: Fig. 3 demonstrates level lines of Φ_n. The minimum point (E_n^*, η_n^*) of Φ_n (Table 1, lines 4 and 5), bringing a solution to the inverse problem was found by a modified conjugate-gradient method [23].

Approximation of the data in Table 1 (line 4) gives the relationship of Young modulus versus temperature

$$E(T) = E_0 \exp(-\alpha T/T_0), \tag{3}$$

where $T_0 = 20$ °C, $E_0 = 647.9$ MPa and $\alpha = 0.384$, the relative error being 19%.

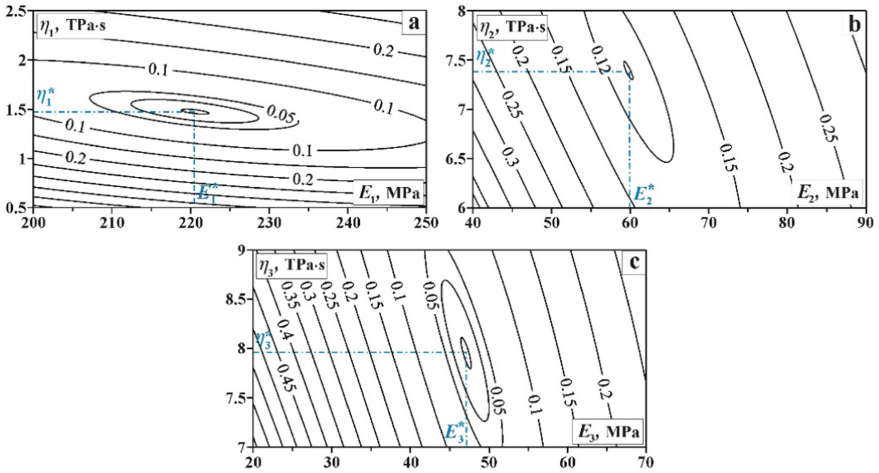

Fig. 3. Level line of objective functions: Φ_1 (a); Φ_2 (b); Φ_3 (c).

It is known [24, 25], that permeability k and porosity m of rocks are related through an empirical law

$$k \cong m^{3/2} \tag{4}$$

and m depends on mean normal stress σ [26]

$$m(\sigma) = m_0 \exp(-\sigma/K), \tag{5}$$

where K – bulk modulus, positive values of σ correspond to compression. Given $3K = E/(1-2v)$ (v – Poisson ratio), it is possible to find the relationship of permeability vs. stresses and temperature from (3), (4), and (5)

$$k(T) = k(T_0)\exp\left[\frac{9(1-2v)\sigma}{2E_0}(\exp(\alpha) - \exp(\alpha T/T_0))\right], \tag{6}$$

value $k(T_0)$ can be determined by standard procedures [27, 28].

3 Experimental Determination of Stress–Permeability Relationship in Granular Geomaterials

The gas-hydrate reservoirs are usually granular [29] or weakly consolidated [30] media, which poroperm properties depend on grain-size composition, porosity, packing and other characteristics [31–33]. The stress state of well environment, packing of a granular matter, and, as a consequence, poroperm properties suffer changes as soon as a producing horizon is exposed and gas-hydrates production is launched. A good deal of laboratory [34–38] and field [12, 39, 40] data is stored on the relationship of rock

(mainly oil-bearing rock) permeability k versus stresses. Experimental data used to be approximated by exponential function [13, 14]

$$k(\sigma_e) = k_0 \exp(-\beta\sigma_e), \tag{7}$$

where $\sigma_e = p - \sigma$ is effective stress, p is fluid pressure, β is empirical coefficient. For rocks of 15–20% porosity $\beta \cong 0.001 - 0.01\,\text{MPa}^{-1}$. Publications containing similar test data on granular media are much scarce in number [41, 42]. However consideration of permeability–stress relationship of type (7) in multiphysical models, describing deformation and mass transfer in a near well zone [43], appreciably influences hydrodynamic and electromagnetic fields and therethrough GIS data inversion results when estimating potential productivity [44].

In the present paragraph, the approach to determine the relationship of granular material permeability versus stresses is substantiated theoretically and evaluated on a physical model.

3.1 Experimental Design and Test Procedure

A measurement cell is a polyurethane sleeve of parallelepiped shape of $l = 105$ mm in length, $h = 30$ mm in width and height with end closed with metal flanges with connectors to a measurement system (Fig. 4). The cell is filled with calibrated sand of 160–250 μm in size, 1650 kg/m^3 of bulk density and 0.165 kg of total weight. The sand was subjected to the maximum consolidation in the wetted state and follow-on drying in the sleeve. The vertical stress S_V was individually applied by means of a loading device to every of three b_1, b_2, b_3 sections of the top edge under control of stress gauges S_1, S_2 and S_3 (Fig. 5). The side edge $x = l$ was under the constant air pressure $p = p_i$, on the opposite edge $p = p_0$ (p_0 – atmosphere pressure); the flow rate was measured in the stationary filtration mode.

Flow rate Q_0 was recorded at $p_i = 2.0, 2.2, \ldots, 3.0$ bar for the initial packing. Stress $S_V = 9$ bar was applied at section b_1; flow rates $Q_{11}, \ldots, Q_{16}$ were measured at the same values of p_i, next section b_2 was loaded and finally the load was applied to section b_3. The relative test values of $\bar{Q}_{in} = Q_{ni}/Q_0$ are summarized in Table 2.

The cell was shaked before every next series of measurements. The initial filtration characteristics of the test packing were controlled by measuring of flow rate $Q_0(p_i)$. Then the loading of sections in the top edge of the physical model was repeated in the above sequence with flow rate measurements: the data on $S_V = 10.5$ and 12 bar are cited in Tables 3 and 4, respectively.

3.2 Model of Experiment

The stationary filtration in the cell was described by a 1D model, including continuity equation

$$div\vec{V} = 0 \tag{8}$$

and Darcy law

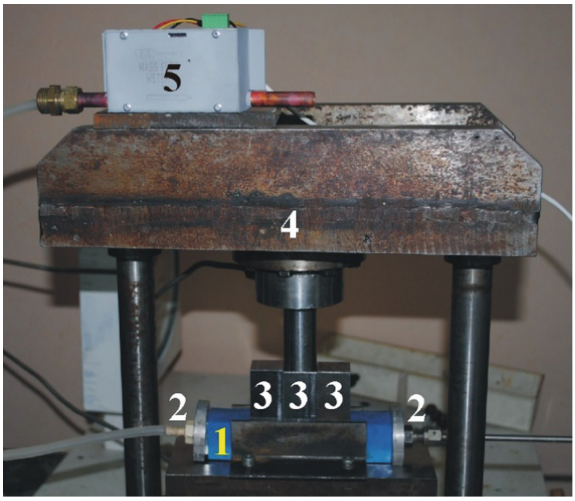

Fig. 4. Test bench: 1–cell; 2–flanges; 3–punches; 4–loading device; 5–flowmeter.

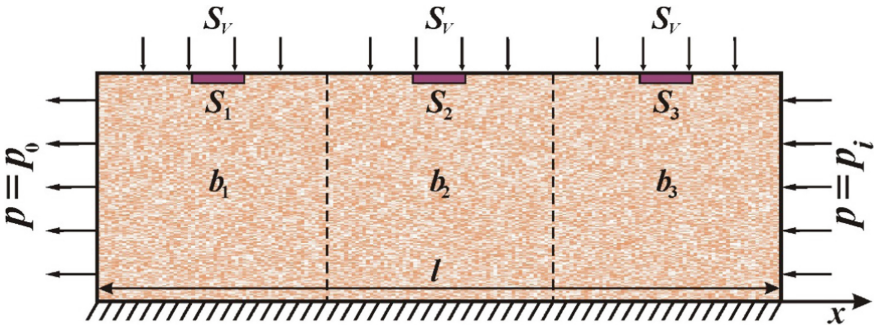

Fig. 5. Experimental design and boundary conditions of the model.

Table 2. Relative flow rate under $S_V = 9$ bar

i	p_i, bar	Q_0, cc/s	Section of loading		
			b_1	b_1, b_2	b_1, b_2, b_3
			$n = 1$	$n = 2$	$n = 3$
			$\bar{Q}_{in}$		
1	2.0	123	1.031	0.894	0.715
2	2.2	154	1.089	0.913	0.717
3	2.4	208	1.074	0.907	0.736
4	2.6	224	1.149	0.925	0.758
5	2.8	266	1.123	0.934	0.823
6	3.0	307	1.174	0.982	0.835

Table 3. Relative flow rate under $S_V = 10.5$ bar

i	p_i, bar	Q_0, cc/s	Section of loading		
			b_1	b_1, b_2	b_1, b_2, b_3
			$n = 1$	$n = 2$	$n = 3$
			$\bar{Q}_{in}$		
1	2.0	121	1.046	0.794	0.649
2	2.2	150	1.056	0.826	0.685
3	2.4	205	1.044	0.834	0.688
4	2.6	223	1.077	0.854	0.718
5	2.8	265	1.099	0.882	0.724
6	3.0	305	1.122	0.907	0.746

Table 4. Relative flow rate under $S_V = 12$ bar

i	p_i, bar	Q_0, cc/s	Section of loading		
			b_1	b_1, b_2	b_1, b_2, b_3
			$n = 1$	$n = 2$	$n = 3$
			$\bar{Q}_{in}$		
1	2.0	120	1.002	0.743	0.627
2	2.2	147	1.011	0.774	0.639
3	2.4	204	1.018	0.784	0.641
4	2.6	222	1.022	0.792	0.657
5	2.8	264	1.057	0.797	0.661
6	3.0	305	1.073	0.866	0.692

$$\vec{V} = -k\nabla p/\mu, \tag{9}$$

where $\vec{V} = (w, 0, 0)$, w is velocity in x direction (Fig. 5), μ is gas viscosity, k is permeability, depending on effective stress under (7), p is pressure. System (7)–(9) is reduced to equation

$$\frac{\partial}{\partial x}\left(\frac{k_0}{\mu} e^{\beta(\sigma - p)} \frac{\partial p}{\partial x}\right) = 0 \tag{10}$$

with boundary conditions (Fig. 5)

$$p(0) = p_0,\ p(l) = p_i. \tag{11}$$

Solution of system (10), (11) is

$$p(x) = \frac{1}{\beta} ln\left[e^{\beta p_0} + \left(e^{\beta p_i} - e^{\beta p_0}\right) G(x,\beta)/G(l,\beta)\right], \tag{12}$$

$G(x,\beta) = \int_0^x e^{\beta\sigma(\xi)} d\xi$, $\sigma(\xi)$ is distribution of mean normal stress within interval $[0, l]$. In the case under consideration σ is a piecewise-constant function, in particular, if a load is applied at section b_1, then $\sigma(\xi) = S_V Z(l/3 - \xi)/3$ (Z being Heaviside step function). It should be note that at $\beta \to 0$ from (12) it follows

$$p(x) = p_0 + (p_i - p_0)x/l.$$

Using (12), it is possible to determine a flow rate at $x = 0$

$$Q(p_i,\beta) = Q_0 F(p_i,\beta),$$
$$Q_0 = \frac{k_0 h^2}{\mu}\frac{p_i - p_0}{l}, \quad F(p_i,\beta) = \frac{\exp(\beta p_i) - \exp(\beta p_0)}{\beta(p_i - p_0)}\frac{l}{G(l,\beta)}$$

thereto Q possesses the following properties

$$\lim_{p_i \to p_0} Q(p_i,\beta) = 0 \quad \lim_{\beta \to 0} Q(p_i,\beta) = Q_0.$$

Level lines $F(p_i,\beta)$ at $S_V = 6$ bar and different loading schemes n are shown in Fig. 6 in dimensionless coordinates $(p_i/p_0, \beta p_0)$. It is explicit that pressure p_i at which $F > 1$ is observed at any β values; it should be considered as a consequence of (7): provided $p > \sigma$, then permeability exceeds initial value k_0.

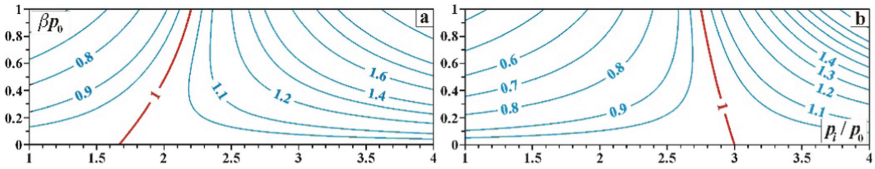

Fig. 6. Level lines of F: $n = 2$ (a); $n = 3$ (b)

3.3 Interpretation of the Experimental Data

Let assess empirical parameter β in terms of test results on relative flow rate $\bar{Q}_{in}$ under different loading schemes n and pressure p_i (Tables 2, 3, and 4). To do this, let consider the objective function

$$\Psi(\beta) = \frac{\sqrt{18\sum_{n=1}^{3}\sum_{i=1}^{6}\left[F(p_i,\beta) - \bar{Q}_{in}\right]^2}}{\sum_{n=1}^{3}\sum_{i=1}^{6}\bar{Q}_{in}}$$

represented a relative discrepancy between theoretical and test values of flow rate. The minimum points of Ψ are required β, cited in Table 5 for different stress values S_V. The

tendency turned out is though insignificant, but reduction in parameter β in (7) with growth of stresses in a granular medium alternatively to the case with rocks.

Table 5. Parameter β in (7) from the experimental data

S_V, bar	β_*, 1/bar	Δ, %
9.0	0.215	4.5
10.5	0.198	6.9
12.0	0.189	5.6

$\Delta = \Psi(\beta_*)$ – relative error

Figure 7 demonstrates the new-obtained relationships $F(p_i, \beta)$ at $\beta = \beta_*$, digits nearby the lines indicate the model-loading schemes; circles are test data.

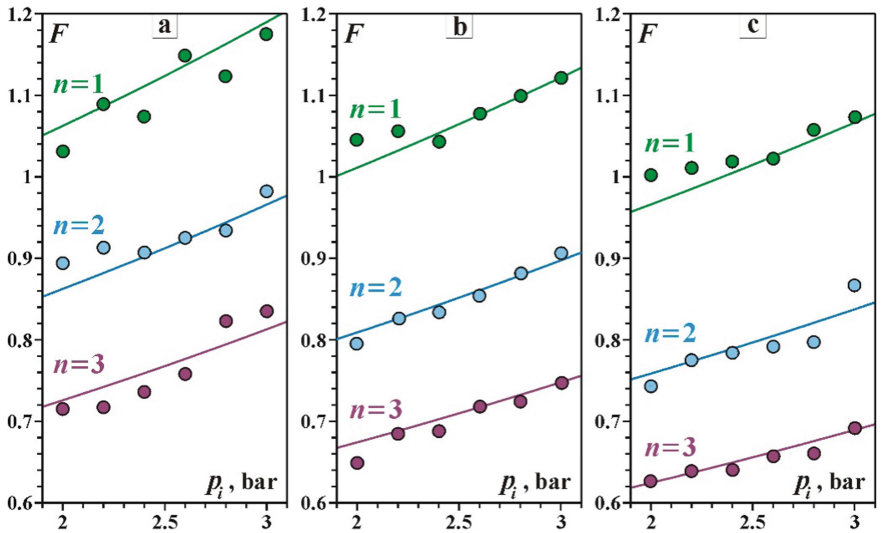

Fig. 7. Functions $F(p_i, \beta)$: $S_V = 9$ bar (a); $S_V = 10.5$ bar (b); $S_V = 12$ bar (c)

It is essential to lay emphasis that the new-proposed method enables to determine parameter β in empirical relationship (7) disregarding a viscosity of a fluid used in the tests and initial permeability of a packing practiced for a granular geomaterial.

4 Analysis of Well Output Characteristics Under Stress-Dependent Permeability and Thermal Treatment of Oil-Bearing Formation

A rise of temperature in a production bed leads to reduction in viscosity μ [19, 44, 45] and growth of compressibility C [46] of oil, and a fall of the matrix bulk module K (given that kerogen content being high) along with accompanying decline in permeability. Let analyze the effect of the above factors on metering characteristics of a well in terms of an axis-symmetric model of a fracture-porous rock mass [47]. The effective compressibility of the oil-filled formation can be evaluated as

$$C_e = m_0 C + (1 - m_0)/K, \tag{13}$$

where K is calculated by (6). In Table 6 the laboratory test data on Bazhenov highly-viscous oil at different temperatures are reported in cursive [45, 46].

Table 6. Viscosity and compressibility of oil at different temperatures.

T, °C	20	40	50	60	80	100	120	150
μ, Pa · s	3.11	***2.47***	***2.06***	***1.74***	***1.44***	1.07	0.82	0.55
$10^9 C$, Pa^{-1}	0.91	***1.28***	1.45	***1.67***	***2.09***	***2.64***	3.29	4.76

The present data are approximated with exponential functions:

$$\mu(T) = \mu_0 \exp(-\delta_1 T/T_0) \tag{14}$$

($\mu_0 = 4.064$ Pa · s, $\delta_1 = 0.266$, relative error $\Delta = 3.4\%$) and

$$C(T) = C_0 \exp(\delta_2 T/T_0) \tag{15}$$

($C_0 = 0.797 \cdot 10^9 \text{Pa}^{-1}$, $\delta_2 = 0.238$, $\Delta = 1.5\%$), which are used to calculate the rest values of μ and C in Table 6.

Let apply the thermal treatment to an oil-bearing bed within an external reservoir boundary (for example, by steam injection [48]); constant temperature T_s is gained. Introduce empirical relationships (13), (14), and (15) (Case I) and next additionally (6) (Case II) into the poroelastic model of borehole environment [16, 47] and simulate an annual oil production volume V.

The computation is based on routine deformation and poroperm properties of a productive oil bed [3, 49], occurring at 2 km depth. Figure 8a demonstrates time variation of V at different temperatures T_s (in relation to the maximum value V_{max} at $T_s = 150°\text{C}$) in terms of the model (Case I). Figure 8b shows the same function, but computed with regard to variations in permeability under (3) (Case II). It is explicit that the selected numerical parameters of the geomechanical-hydrodynamic model can really give the double overestimated production rate prediction in the case of

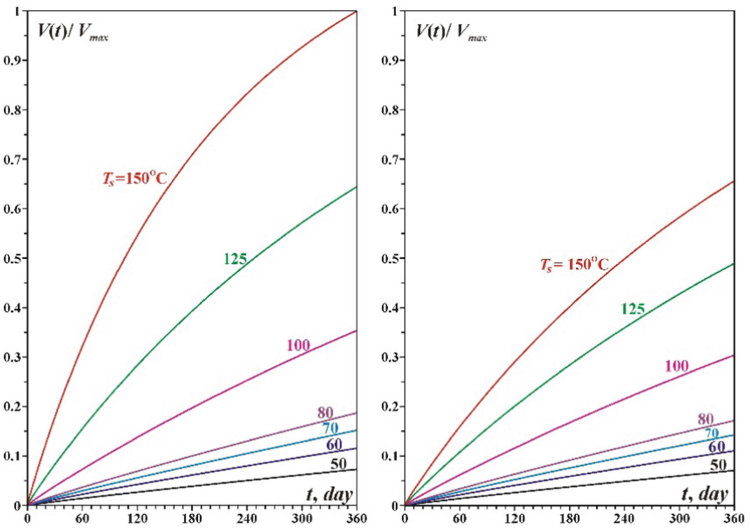

Fig. 8. Annual oil production volume V: Case I (a); Case II (b)

disregarding the thermal effect on elastic characteristics of an oil-bearing bed, viz., the resultant permeability decline as a consequence.

5 Conclusion

The processes enabling to establish a quantitative relation between filtration properties of oil-bearing beds consisting of granular and high-organic rocks versus stresses and temperature are theoretically justified and tested. The processes rest on solving the coefficient inverse problems using test data obtained at original laboratory test facilities. The comparative analysis of metering well characteristics revealed that a disregard of the empirical permeability–effective stress relationships might lead to appreciably overestimated oil production prediction.

Acknowledgement. The investigations was partially supported by the Russian Foundation for Basic Research: Project No. 16-05-00573 (paragraphs 2&4) and Project No. 18-05-00830 (paragraph 3).

References

1. Speight, J.G.: An Introduction to Petroleum Technology, Economics, and Politics. Wiley, New York (2011)
2. Dake, L.P.: The Practice of Reservoir Engineering. Elsevier, The Netherlands (2001)
3. van Golf-Racht, T.D.: Fundamentals of Fractured Reservoir Engineering. Elsevier, Amsterdam (1982)

4. Rutqvist, J., Wu, Y.-S., Tsang, C.-F., et al.: A modeling approach for analysis of coupled multiphase fluid flow, heat transfer, and deformation in fractured porous rock. Int. J. Rock Mech. Min. Sci. **39**, 429–442 (2002)
5. Coussy, O.: Mechanics and Physics of Porous Solids. Wiley, New York (2010)
6. Nie, R.-S., Meng, Y.-F., Jia, Y.-L., et al.: Dual porosity and dual permeability modeling of horizontal well in naturally fractured reservoir. Transp. Porous Media **92**(1), 213–235 (2012)
7. Zhou, X., Ghassemi, A.: Finite element analysis of coupled chemo-poro-thermo-mechanical effects around a wellbore in swelling shale. Int. J. Rock Mech. Min. Sci. **46**(4), 769–778 (2009)
8. Zhuang, X., Huang, R., Liang, C., Rabczuk, T.: A coupled thermo-hydro-mechanical model of jointed hard rock for compressed air energy storage. Mathematical Problems in Engineering, ID 179169 (2014)
9. Wu, K., Olson, J.E.: Simultaneous multifracture treatments: fully coupled fluid flow and fracture mechanics for horizontal wells. SPE J. **20**(02), 337–346 (2015)
10. Wu, Y.-S.: Multiphase fluid flow in porous and fractured reservoirs. Elsevier, Amsterdam (2016)
11. Yeltsov, I.N., Nazarov, L.A., Nazarova, L.A., et al.: Logging interpretation taking into account hydrodynamical and geomechanical processes in an invaded zone. Dokl. Earth Sci. **445**(2), 1021–1024 (2012)
12. Daigle, H., Rasromani, E., Gray, K.E.: Near-wellbore permeability alteration in depleted, anisotropic reservoirs. J. Petrol. Sci. Eng. **157**, 302–311 (2017)
13. Zoback, M.D., Nur, A.: Permeability and effective stress. Bull. Am. Assoc. Petrol. Geol. **59**, 154–158 (1975)
14. Ma, J.: Review of permeability evolution model for fractured porous media. J. Rock Mech. Geotech. Eng. **7**(3), 351–357 (2015)
15. Nazarova, L.A., Nazarov, L.A., Golikov, N.A.: Assessment of rheological properties of bazhenov formation by thermobaric test data. J. Min. Sci. **53**, 434–440 (2017)
16. Yeltsov, I.N., Nesterova, G.V., Sobolev, A.Y., Epov, M.I., Nazarova, L.A., Nazarov, L.A.: Geomechanics and fluid flow effects on electric well logs: multiphysics modeling. Russ. Geol. Geophys. **55**(5–6), 775–783 (2014)
17. BP Statistical Review of World Energy (2018)
18. Zapivalov, N.P.: Geological and technological peculiarities in development of difficult mineral resources. Oil Ind. **6**, 57–59 (2005)
19. Butler, R.M.: Thermal Recovery of Oil and Bitumen. Prentice-Hall, Englewood Cliffs (1991)
20. Bennion, D.B., Ma, T., Thomas, F.B. et al.: Laboratory procedures for optimising the recovery from high temperature thermal heavy oil and bitumen recovery operations. In: Petroleum Society's 8th Canadian International Petroleum Conference, paper 2007–206, Canada (2007)
21. Cristescu, N.: Elastic-viscoplastic constitutive equation for rock. Int. J. Min. Sci. Geomech. Abs. **24**(5), 271–282 (1987)
22. Wu, L., Zuo, Q., Lu, Z.: Study on the constitutive model of visco-elasticity-plasticity considering the rheology of rock mass. Adv. Mater. Res. **639–640**, 567–572 (2013)
23. Nazarov, L.A., Nazarova, L.A., Karchevsky, A.L., Panov, A.V.: Estimation of stresses and deformation properties of rock masses which is based on the solution of an inverse problem from the measurement data of the free surface displacement. J. Appl. Ind. Math. **7**, 234–240 (2013)
24. Dullien, F.A.L.: Porous Media: Fluid Transport and Pore Structure. Academic Press, New York (1979)
25. Carman, P.C.: Flow of Gases Through Porous Media. Butterworths Scientific Publications, London (1956)
26. Shchelkachev, V.N.: Selected Works in Two Volumes, vol. 1. Nedra, Moscow (1990)
27. GOST N. 26450.2-85. Rocks. Method for determination of absolute gas permeability coefficient by stationary and non-stationary filtration (1985)

28. Vafai, K.: Handbook of Porous Media, 2nd edn. Taylor & Francis Group, USA (2005)
29. Istomin, V.A., Yakushev, V.S.: Gas Hydrates in Natural Conditions. Nedra, Moscow (1992)
30. Isaeva, O.A., Bruzhes, L.N., Vavilin, V.A., et al.: Lithology, mineralogy and pore space of the ryabchik-type AV1 horizon in the Urevskoe oilfield. In: Sedimentary Basins, Sedimentation and Post-Sedimentation Processes in Geological History. In: Proceedings of VII All-Russian Lithological Conference, vol. 1, pp. 388–392. INGG SO RAN, Novosibirsk (2013)
31. Urumovic, K., Urumovic, Sr.K.: The effective porosity and grain size relations in permeability functions. Hydrol. Earth Syst. Sci. Discuss. **11**, 6675–6714 (2014)
32. Knackstedt, M.A., Duplessis, J.P.: Simple permeability model for natural granular media. Geophys. Res. Lett. **23**(13), 1609–1612 (1996)
33. Kuhn, M.R., Sun, W., Wang, Q.: Stress-induced anisotropy in granular materials: fabric, stiffness, and permeability. Acta Geotech. **10**(4), 399–419 (2015)
34. Holt, R.M.: Permeability reduction induced by a nonhydrostatic stress field. SPE Formation Eval. **5**, 444–448 (1990)
35. Heller, R., Vermylen, J., Zoback, M.: Experimental investigation of matrix permeability of gas shales. Bull. Am. Assoc. Petrol. Geol. **98**(5), 975–995 (2014)
36. Roi, R., Paredes, X., Holtzman, R.: Reactive transport under stress: Permeability evolution in deformable porous media. Earth Planet. Sci. Lett. **493**, 198–207 (2018)
37. Pan, Z., Connell, L.D.: Modelling permeability for coal reservoirs: a review of analytical models and testing data. Int. J. Coal Geol. **92**, 1–44 (2012)
38. Geng, Y., Tang, D., Xu, H., et al.: Experimental study on permeability stress sensitivity of reconstituted granular coal with different lithotypes. Fuel **202**, 12–22 (2017)
39. Rhett, D.W., Teufel, L.W.: Effect of reservoir stress path on compressibility and permeability of sandstones. In: SPE Annual Technical Conference and Exhibition. SPE Paper No. 24756, Washington DC (1992)
40. Randall, M.S., Conway, M., Salter, G., Miller, S.: Pressure-dependent permeability in shale reservoirs implications for estimated ultimate recovery. In: AAPG Search and Discovery Article N 9012.2011, AAPG Hedberg Conference, Austin, Texas (2010)
41. Chapuis, R.P., Gill, D.E., Baass, K.: Laboratory permeability tests on sand: influence of the compaction method on anisotropy. Can. Geotech. J. **26**(4), 614–622 (1989)
42. Wong, R.C.K.: Strain-induced anisotropy in fabric and hydraulic parameters of oil sand in triaxial compression. Can. Geotech. J. **40**(3), 489–500 (2003)
43. Nazarova, L.A., Nazarov, L.A., Epov, M.I., Eltsov, I.N.: Evolution of geomechanical and electro-hydrodynamic fields in deep well drilling in rocks. J. Min. Sci. **49**, 704–714 (2013)
44. Farouq Ali, S.M., Jones, J.A., Meldau, R.F.: Practical heavy oil recovery. Mont Resour Inc., Bakersfield (1997)
45. New Chemist's and Engineer's Handbook, V.1, Basic properties of inorganic, organic, and elementary-organic compounds. Mir i Semiya, Moscow (2002)
46. Bilinkin, G.P., Kuvandikov, I.Sh.: Dependence of volume coefficient, coefficient of compressibility, density of deep–subsided bed oils from pressure, temperature, composition and gas content. Geology of Oil and Gas, 9 (1992)
47. Nazarova, L.A., Nazarov, L.A.: Evolution of stresses and permeability of fractured-and-porous rock mass around a production well. J. Min. Sci. **52**, 424–431 (2016)
48. Mozaffari, S., Nikookar, M., Ehsani, M.R., et al.: Numerical modeling of steam injection in heavy oil reservoirs. Fuel **112**, 185–192 (2013)
49. Nazarova, L.A., Nazarov, L.A.: Evolution of hydrodynamical and stress fields in near-well zone in fractured porous media. In: Proceedings of the 6th Biot Conference on Poromechanics 6, Paris, pp. 287–294 (2017)